FULL LENGTH PAPER

INCEPTION OF CASING WALL FLOW INSTABILITIES AND DOWNSTREAM FLOW EVOLUTION IN SUBSONIC AXIAL COMPRESSOR ROTORS AT HIGH ROTOR STAGGER ANGLES

P.V. Ramakrishna and M. Govardhan
Thermal Turbomachines Laboratory
Department of Mechanical Engineering
Indian Institute of Technology Madras
Chennai-600 036, India
Email : gova@iitm.ac.in

Abstract

Two critical aspects of the casing wall flow structure in a subsonic axial flow compressor are studied in this paper: flow mechanism leading to stalling at different stagger angle configurations; and the effect of tip leakage flows on these flow phenomena. In some of the previous works, casing wall flow instabilities similar to the ones discussed in the present paper were reported, typically for high stagger angle rotor designs. However under what conditions flow tends to take such shapes were not discussed in detail. This work attempts to address this through a detailed numerical study on unswept and forward swept rotors, for different stagger angle settings, and for varied levels of rotor tip gaps. Three candidate rotors (unswept, 20° true swept, 20° axially swept) are studied with three tip clearances (0.0%, 0.7%, and 2.7% of the blade chord) for three stagger angle changes (0°, +3° and +5°). Stagger angle is found to have significant effect on suction surface flow separations. Tip clearance is observed to be critical on the inception of casing wall flow instabilities, especially at higher stagger angles. Hub endwall flow structure and the downstream flow evolution are also discussed in the paper.

Keywords: Stagger angle, Tip clearance, Blade sweep, Flow separation, Total and static pressure coefficients, Axial velocity coefficient

Nomenclature

ch = Chord (mm)
C_m = Axial velocity (m/s)
C_r = Radial velocity (m/s)
C_u = Tangential velocity (m/s)
LE = Leading edge
P = Static pressure (N/m^2)
PS = Pressure surface
Po = Total pressure (N/m^2)
r = Radius (m)
S = Blade spacing (m)
SS = Suction surface
TE = Trailing edge
U_t = Tip speed (m/s)
W = Relative velocity (m)
x = Non-dimensionalized streamwise location
y = Tangential distance (m)
α = Absolute flow angle (deg)
β = Blade angle (deg)
γ = Stagger angle (deg)
ϕ = Flow coefficient (C_m/U_t)
ψ_o = Total pressure rise coefficient, $\left[\psi_o = \left(\frac{P_{02} - P_{01}}{\rho\, U_t^2}\right)\right]$
λ = Sweep angle (deg)
v = Dihedral angle (deg)
τ = Tip gap (m)

Subscripts

* = Design
1 = Inlet to rotor
2 = Exit of rotor

Paper Code : V66 N2/819-2014. Manuscript received on 27 May 2013. Reviewed, revised and accepted as a Full Length Contributed Paper on 29 Apr 2014

3 = Exit of stator
rel = Relative frame
t = Tip

Superscripts

- = Pitchwise mass averaged
= = Pitchwise and spanwise mass averaged

Introduction

Compressor casing endwall flow structure is very complex with the prevailing tip leakage flows, low energy fluid attached to the blade boundary layer, annulus wall boundary layer and secondary flows; and interactions of these flows with the main flow result in an intricate flow structure in this region. Towards the stall limit, severe separations in this region, tip leakage flow driven by high loading conditions and their interactions result in further flow disturbances leading to unstable operation of a compressor.

In their previous works the authors have discussed how forward sweeping of rotors in low speed compressors mitigates endwall boundary layer growth and other beneficial effects combined with tip leakage flows at the casing endwall [1]. Flow separations leading to stalling of the candidate compressor were discussed and various effects of sweep and tip clearance on these phenomena were reported. A detailed study on tip leakage phenomena with considerations on various compressor design/operating parameters is made in Ramakrishna and Govardhan [2]. This work reports that the origin of tip leakage vortex shifts downstream along the chord, with increased flow coefficient and increased tip gap (in contrary to what was reported earlier by Yoon et al. [3]). In particular, flow coefficient was reported to have a predominant effect on the location of the pressure trough on the tip surface, where the vortex tends to originate. The sensitivity of rotor tip sections to local pressure distributions was also reported in [2] for different rotor sweep configurations.

Later in another study [4] the authors have reported the effect of high rotor stagger angles on tip leakage phenomenon in the candidate subsonic compressor. At high stagger angle settings, flow separations critical to the compressor stalling were reported to occur at upstream rotor suction surface. Small tip gap was reported to have positive effects for certain stagger angle increments owing to beneficial interaction of leakage flows with the local flow field; however, severe performance loss was reported at high stagger angle settings employed with large tip clearances. One conclusion of this work critical to the present paper is that the flow was reported to leak in a more "axially reversed" fashion through the tip gap at high stagger angles.

Thus, two important aspects of the tip endwall flow are worth a keen attention from the past observations of the authors as well as from the earlier knowledge on compressor endwall flow structures:

- What flow mechanism causes rotor stall at different stagger angle configurations?
- What is the effect of tip leakage flows on this particular mechanism?

An attempt is made in this paper to give an insight into the flow structure at the tip-endwall regions and to provide reasonable explanations to the aforesaid questions. This is the prime focus of the paper. Hub wall flow structure and how these endwall flow features evolve as the flow progresses to downstream stages will also be discussed in the final sections to complement, however, in less detail.

Literature on Endwall Flow Instabilities

Flow in an axial compressor can breakdown into either rotating stall or surge. In either case, the unstalled compressor first becomes unstable as the flow rate is reduced and as a result of stall the flow pattern is altered into one of these forms. In a compressor operating at unstalled conditions, the inception of instabilities would make the operation unstable and would lead to stall with further reduction of flow. A stable operating process known as rotating stall occurs after the machine has stalled.

Once a flow becomes nonuniform, there are many degrees of freedom and the flow can establish itself in many different ways. In consequence, flow that is stalled (in the sense that this takes for rotating stall in compressors) can exhibit many different arrangements. The compressor will be unstable at the instant before it moves from being unstalled to being in rotating stall; similarly, for a compressor in rotating stall, there will be an instantaneous condition of instability as the throttle is opened and it moves from stalled to unstalled. The stalled condition, however, is normally very stable, Cumpsty (Discussion on März, et al. [5]).

Rotating instability, in general, is a phenomenon that occurs in the tip flow region of axial compressor stages during stable operation. It is observed in highly staggered rotors with significant tip clearance and is strongest at high-load operating points towards the stall limit. Mailach, et al. [6] observed rotating instabilities near the stability limit in an axial compressor (tip stagger = 40.5° and with a relatively large tip gap) originating from the fluctuating blade tip vortex, as responsible for the excitation of high amplitude rotor blade vibrations and noise generation. März, et al. [5] presented one of the forms of rotating instability. A vortex structure was reported to form near the leading edge plane as a result of interaction among the classical tip clearance flow, axially reversed endwall flow, and the incoming flow. The vortex was reported to travel from the suction side to the pressure side of the passage at half of the rotor speed. The formation and unsteady movement of this vortex was considered to be the main cause of unsteadiness when rotating instability develops. They observed the rotating instabilities most clearly near the maximum loading conditions for high tip gap levels. They claimed that the high unsteadiness near the casing endwall is mainly due to the unsteady movement of the tip clearance vortex which is amplified with increase in the tip gap, also reported by Zierke, et al [7]. März, et al. [5] observed rotating instability alone near the design point operation, rotating instability plus rotating stall when approaching the stall line, and rotating stall alone when the machine is throttled further.

Hoying, et al. [8] carried out computational simulations to study the role of blade passage flow structures with short length scale (or spike) type of stall inception on the low speed version of the GE E^3 compressor (Wisler [9]), which was experimentally observed to exhibit such short length scale type of stall inceptions (Silkowski [10]). This kind of stall inception was found to be fundamentally different from the long length scale modal stall. This process is linked to the behavior of the blade passage flow field structure, specifically the tip leakage vortex, in contrast to the modal stalling case where a description of the flow structure within the blade passage is not required for a useful description of rotating stall inception and development. The flow field was observed to become unstable when the leakage vortex trajectory is aligned with the blade leading edge plane (tangential), to initiate stall.

Davis and Yao [11] through their investigations on the transonic NASA Stage35 compressor stage reported another form of interaction of the leakage flow with the secondary flows prevailing at the casing regions that leads to stall. Two vortex structures were observed at the tip in this compressor passage, the first corresponds to the classic leading edge tip vortex and the second vortex corresponds to a merging of the tip flow with a vortex that lies along the suction surface caused by the shock/blade boundary layer interaction. Towards the stall point, the second vortex structure had grown in size and blockage.

Another form of tip leakage flow interaction that triggers tip stall in transonic compressors was reported by Suder and Celestina [12]. These researchers explained the cause for the second vortex observed at the trailing edge of the blade as the supersonic flow near the blade leading edge when encounters the downstream adverse pressure gradients, would result in radial migration of fluid along the blade suction surface. This fluid climbing up the suction surface when encounters the leakage flow at the blade tip rolls up into the second vortex. Through a parametric study of tip clearance, they concluded that the formation of the second vortex is not related to the strength of the clearance flow but rather is due to the secondary flows along the blade suction surface that result from operating at an off design conditions in a transonic compressor.

This second vortex pattern described in the literature in all these earlier studies is very much similar in its nature to the one (will be discussed) in the present study as blade boundary layer separation vortex near the trailing edge of the blade. Note that the effect of speed (part speed/design speed) as observed by Suder and Celestina [12] would be opposite in subsonic compressor environments. The effect of high rotor speed would promote high centrifugation of boundary layer on the suction surface and lead to much stronger separation vortex near the trailing edge. On the other hand, phenomenon responsible for the sudden drop in rotor pressure rise due to the rapid increase in blockage when the upstream edge of the rotor tip vortex becomes co-planar with the leading edge plane of the rotor at the tip was observed and reported by various researchers [13-16].

Thus, in the light of the available literature on the endwall flow instabilities in compressors, critical features of the casing endwall flow triggering stall can be listed out as:

- Tip leakage flow, its intensity, extent, unsteady behavior, trajectory; and the location on the blade tip where it rolls up in the form of a leakage vortex

- Blade boundary layer separation vortex (or second vortex) observed at the blade tip trailing edge
- Blockage caused by the tip leakage vortex at the inlet near the casing

Stagger angle and tip gap levels are found to influence the above features to a greater extent. They also dictate the form the flow takes under various flow conditions containing tipward flow instabilities; for the fact that the nature of the instabilities itself is dictated by these factors.

Present numerical work reports the effects of stagger angle variation and tip clearance in subsonic axial compressor rotor passages leading to stalling. Towards drawing some general conclusions, some results will be reported for two forward swept (20° TCS and 20° AXS) rotors, in which some flow results look much apparent.

TCS refers to tip chordline sweeping (also known as true sweeping) and AXS refers to axial sweeping. More details of these rotors can be found in Ramakrishna and Govardhan [17]. Note that the baseline unswept rotor (UNS) was deliberately designed to have a thick boundary layer development on the suction surface that gets centrifuged towards tip, so that effect of sweeping on this flow mechanism can be seen explicitly. Forward swept rotors mitigate such centrifugation result in reduced endwall boundary layer growth and other performance benefits (as mentioned in the initial sections of the paper).

It is not unusual to vary the stagger angle (rotating the whole blades about their mounting axes to close/or open the rows) in a controlled fashion to alleviate the stage mismatching at off design conditions. The role of stagger angle variation is studied by considering three different stagger angle settings: $\Delta\gamma = 0°$, $\Delta\gamma = +3°$ and $\Delta\gamma = +5°$, measured from the designed value. Stagger angle convention followed in this study is shown in Fig.1. Positive sign signifies that the stagger angle is increased in the study which implies that at high stagger angles, the passage is closed by rotating the blade about the mounting axis.

The high stagger setting of $\Delta\gamma = +5°$ was so chosen for the following reasons: In the baseline UNS rotors, when operating mass flow is reduced to the stall mass flow ($\phi = 0.50$), the incidence is found to increase by 5° (approx.) all along the span. Hence it was decided to stagger the blade by $\Delta\gamma = +5°$ so that the design incidence is felt at the stall flow coefficient. Also, with respect to the tip, the highly staggered blade configurations in the existing literature (e.g., [6]) use tip stagger of about 40°; and at $\Delta\gamma = +5°$, the tip stagger in the studied rotors already becomes 50°. Such severely high tip stagger angles are found to result in interesting flow features, which will be discussed in the paper.

The Computational Model

The computational domain employed in the computations consists of a rotor followed by a stator row with specifications mentioned in Table-1. Hexahedral grids (typically about 700,000 mesh elements for the rotor and 450,000 elements for the stator) were employed with finest mesh near the walls and within the tip gap for better mesh resolution. Solver utilizes k-ω turbulence modeling; and the solution was second order accurate. Details of the computational methodology adopted in the present work, numerical validation and so forth, have been presented in Ref. [17-19] in detail; and will not be repeated here. High quality hexahedral grids have been employed in the computations. Standard k-ω turbulence model was used with automatic wall function treatment at walls. All the cases were solved till a convergence of 1×10^{-5} is achieved for the RMS residuals with high resolution scheme, which is second order accurate. The self-adaptive high resolution methods are different from the second or higher order schemes in that they handle simulations involving flow discontinuities (such as fluid interfaces and shear layers) by appropriately adjusting the blending factors between accuracy and robustness. Fig.2a shows typical variation of

Table-1 : Specification of the Compressor Stage

Rotational speed	1950	(rpm)
Design mass flow rate	2.725	(kg/s)
Casing diameter	400	(mm)
Hub diameter	200	(mm)
Mean chord (rotor and stator)	75	(mm)
Number of blades (rotor and stator)	12 and 11	--
Aspect ratio based on mean chord	1.33	--
Reynolds number based on the mean chord	$1.26*10^5$	--
de Haller no. at the mean radius (W_2/W_1)	0.74	--
Total efficiency	85%	--

mass and momentum RMS residuals in a solution up to around 300 iterations. While this figure is plotted for baseline stagger angle case ($\Delta\gamma = 0°$) at a low mass flow rate ($\phi = 0.54$) condition, the convergence pattern was found to be similar for various mass flow rates, for the three stagger angle settings studied.

Validation

The simulations have been validated with the reported experimental results [20] on the candidate compressor. CFD results are found to be in good agreement with the experiments. Fig.2b compares the total pressure rise coefficient between experiments vs. CFD at two mass flow rate conditions for the baseline case ($\Delta\gamma = 0°$). More validation results are available in [19].

The next section describes how the stagger angle and tip gap collectively influence the casing wall flow features altering the mechanism of instabilities and casing wall stalling.

Endwall Flow Structure at High Stagger Angles

In light of the original discussion, the following is the focus of the subsequent sections:

- Flow mechanism that causes rotor stall at different stagger configurations
- Effect of tip leakage flows on this particular mechanism

A little insight into the flow physics at the tip-endwall regions would provide the explanations to these points. Figs.3-5 from the present study would facilitate this.

Figure 3 shows the nature of flow separations as modified by the blade stagger angle. At low stagger angle ($\Delta\gamma = 0°$ case), huge amount of separated flow collected from large portions of the blade can be seen to form a core of the corner separation vortex. As the stagger angle is increased, boundary layer flow from the front portions of the blade is separated instantaneously; and another separation is seen towards the tip trailing edge (TE) forming trailing edge separated vortex.

Figure 4 shows the endwall flow field with a static pressure rise coefficient contours at tip regions. It was comprehensively reported in Ramakrishna and Govardhan [2] that the effect of increased tip clearance and increased flow coefficient is to shift the low pressure trough (and the tip clearance vortex formation) to downstream chordwise locations on the blade tip. Stall occurs at low flow coefficients for higher stagger angle configurations. With increasing stagger angle, these phenomena had resulted in early rollup of tip leakage vortex, at the front portions of the blade, very close to the LE at $\Delta\gamma = +3°$, $\phi = 0.43$; and starting from the tip LE at $\Delta\gamma = +5°$, $\phi = 0.38$. Such an early leakage vortex formation has a remarkable effect on the endwall flow field. The major effect would be to cause enormous blockage close to the leading edge causing severe flow incidences. These high flow incidences would in turn lead to inception of flow instabilities and unsteady disturbances. These aspects of flow are evident from the velocity vectors drawn on blade-to-blade plane at a distance of 1.5 mm from the rotor tip for various tip clearances (Fig.5) and will be discussed in the next section. Since these locations are at different distances from the outer casing wall for different tip gap heights, effect of endwall and blade surface boundary layer is embedded in these results. However, as the primary intention is to observe the flow pattern for different cases, this boundary layer influence is not separately assessed.

Another effect at times beneficial, and many times not, is the interaction of the leakage flow with the endwall secondary flows. Tip leakage flow, whether emerged in the form of a leakage vortex at earlier chordwise locations or later, would definitely interact with the local secondary flows. But at higher stagger angles, the interaction is of major concern owing to the nature of these secondary flows (primarily the separated blade boundary layer flows) at higher stagger angles.

Figure 4 also demonstrates that the leakage flow is perpendicular to the chord over most of the tip for the highest stagger and tip clearance case studied ($\Delta\gamma = +5°$, $\phi = 0.38$, $\tau/ch = 2.7\%$). Increasing stagger angle results in more circumferential orientation of the blade. In such case, towards the stall limit, the mass flow rate is also very less: implying that for the same incidence, flow enters the blade (in the relative frame) highly tangentially. Flow leaking through the tip gap perpendicular to the chord, indeed very close to the leading edge (LE) would invariably cause enormous flow blockage at the very entrance to the blade passage. This increases the severity of the flow conditions, as observed from Fig.4 pertaining to the above mentioned case.

Figure 5a shows the velocity vector field on blade-to-blade planes, which are 1.5 mm below the rotor tips,

plotted for the near-stall flow coefficients at the respective stagger angle cases. At $\Delta\gamma = 0°$, separated flow near the TE regions of the tip is seen as axially reversed flow vectors (colored with negative axial velocity coefficient in the contours). This axially reversed flow extends over large circumferential portions of the passage. As a result high blockage zones are seen in the downstream passage regions. With the introduction of a small clearance (τ/ch = 0.7%), distinct zones of flow blockage are observed corresponding to the tip clearance vortex and the separated flow vortex near the TE. In the mid-chord regions, interaction of tip clearance flow is observed to minimize the separations in these regions. Tip leakage vortex and its blockage grows in size with τ/ch = 2.7%. Blockage related to flow separations at the TE are minimum in this case (Fig.5a).

In the same figure, as the stagger angle is increased, pressure gradients in the axial direction increase dramatically owing to small passage area and the low flow rate in the passage (stall point shifts to lower mass flow rates). Therefore the adverse pressure gradients are felt significantly. The axially reversed flow blockage region is observed to increase over large circumferential regions with increasing stagger angles.

Vector flow fields corresponding to the swept rotors are shown in Fig.5b and 5c. The major observations drawn from comparing these flow fields with those observed for the UNS rotor are as follows:

- For the zero clearance case, blockage caused by the axially reversed flow is less severe in both the swept rotors as the severity of separation itself is less in these rotors; the least being observed with the 20° AXS rotor.
- Blockage related to the tip leakage vortex is also less for the swept rotors, again, the least being for the 20° AXS rotor.
- Due to reduced blade boundary layer flow centrifugation and less intensity and severity of the flow separations near the TE with the swept rotors, interaction of the axially reversed flow in these regions with the tip leakage vortex is not observed at the higher stagger, except for the individual case of highest stagger and the highest tip clearance studied ($\Delta\gamma = +5°$, τ/ch = 2.7%). In this case, both the swept rotors showed significant interaction of this type (Fig.5b and 5c). This is due to the large tip gap forming strong tip leakage vortex, close to the blade LE, causing very high blockage near to the LE plane. This made the downstream locations behind the leakage vortex being deprived of flow progression and the separated flow to get upturned towards the frontal portions of the passage. Complete blockage of flow passage at this radial location (blade-to-blade plane at a distance of 1.5 mm from the rotor tip) can be seen in these rotors (more predominantly in the 20° AXS rotor for $\Delta\gamma = +5°$, τ/ch = 2.7%). Evidence of instability similar to an unstable radial vortex can be seen in 20° AXS rotor near the suction surface, very near to the LE of the tip leakage vortex. Instability of this kind is observed in the middle of the passage, close to the edge of the tip leakage vortex in 20° TCS rotor.

März, et al. [5] through their unsteady analysis reported that inception of instability is followed by its unsteady movement in the passage; and this behavior leads to stalling of the compressor. They observed instability very much similar to the ones observed here; and the instability in the form of a radial vortex moved from the suction side of the passage to the pressure side at roughly half the rotor speed. As this vortex moved in the tangential direction, the local pressure field also changed due to the change in blockage.

It should be noted that a steady state analysis may not be completely adequate to fully study the behavior of such instabilities. The flow fields shown in Fig.5 can be considered as snapshots of such phenomena at particular instances.

A further analysis of these flow fields with respect to increasing stagger and increasing tip gap is presented in the following sections.

Flow entering the blade passage gets highly accelerated near the LE portions on the suction surface (Fig.5a). Suction surface evidences peak relative velocity to occur in the front portions of the blade. Flow decelerates on the later portions of the suction surface to achieve the required diffusion towards the exit. In most of the cases, flow leaking from the tip gap encounters the "accelerating" portion of the flow on the suction surface upon spilling out to the adjacent blade passage. These two flows essentially carry the highest velocities available on the particular spanwise blade-to-blade flow field and would encounter each other at widely different angles. This causes the leakage flow to quickly rollup into the leakage vortex

whose trajectory depends on the magnitude of both throughflow and the leakage flow velocities. It is believed that orientation of the leading edge of the leakage vortex dictates the extent of blockage contributed by the leakage vortex. The more circumferential is this leading edge (more co-planar with the blade LE plane), the more is the blockage caused.

From the same figure (Fig.5a), it can be noted that acceleration at the front blade portions on the suction surface occurs at all radial stations, but its encounter with the leakage flow is confined to the near tip sections. At non-zero tip clearances, very high flow velocities near the suction surface at more downstream chord locations can be observed due to the leakage flow. Flow velocities and the chordwise extent of these regions therefore increased with increased tip clearance owing to more leakage. Tip leakage flow spills across the tip aerofoil to the adjacent blade passage, where its encounter with the accelerated flow results in the formation of a vortex in the front portions of the tip, while flow leaking through the downstream portions of the tip would be carried downstream, causing certain extent of blockage, primarily because its direction is different from the meridional direction. This does not contribute much to the pressure loss, though (see discussion on "Total Pressure Loss within the Tip Gap", Ramakrishna and Govardhan [2]). On the other hand, near the TE the leakage flow encounters the centrifuged blade boundary layer flow. Rolling-up of this centrifuged boundary layer flow into a separated vortex is not much promoted by its interaction with the leakage flow, but depends on the degree of centrifugation; as this type of separated vortex is observed with strong boundary layer centrifugation even without clearance at the tip. With increased clearance, distinct zones of blockage due to tip leakage vortex and the blade boundary layer separation vortex near the TE can be observed.

At $\Delta\gamma = +3°$, Various Tip Gaps

At $\Delta\gamma = +3°$, $\tau/ch = 0.0\%$ (Fig.5a), separated flow from the TE portions of the blade can be seen as axially reversed flow similar to the one observed previously with $\Delta\gamma = 0°$. Among the three stagger angle cases, although the nature of blockage corresponding to the separations has been similar on this radial plane, the actual nature of the separations differs (as discussed before, Fig.3). Owing to these differences significant alterations in the endwall flow field are observed when clearance is introduced at the tip.

At $\Delta\gamma = +3°$, $\tau/ch = 0.7\%$ (Fig.5a), formation of leakage vortex occurs at an early chordwise location (close to the tip LE) and causes increased blockage in the front portions of the passage near the casing. Note that the LE of the leakage vortex is becoming more tangential in the passage at higher stagger angles. This blockage at the passage entrance caused by the leakage vortex is found to promote the flow separated from the TE portions to move towards the forward portions of the blade passage. A keen observation of the figure would reveal that the accelerated flow on the front portions of the suction surface when encounters the axially reversed flow, both of these flows revert back to a direction dictated by the magnitude of the respective flows. This was also observed in the case of $\Delta\gamma = 0°$, $\tau/ch = 0.7\%$, but a very noticeable difference in the phenomena can be observed at higher stagger angles, when these flows after reverting back encounter the tip leakage vortex causing a complex interaction leading to a flow instability in these regions. A radial vortex like structure confined to a small radial extent in the near wall regions can be seen (enclosed in a dashed circle, described *I-1* in Fig.5a) to be originated at the corner shaped by the suction surface accelerated flow and the leading edge of the leakage vortex. Such complex flow interaction is promoted by the high adverse pressure gradients and low streamwise flow velocities coupled with highly tangential incoming flow at the higher stagger angles.

When the clearance is increased, at $\Delta\gamma = +3°$, $\tau/ch = 2.7\%$ (Fig.5a), blockage caused by the leakage vortex extends almost to the PS of the adjacent blade in the circumferential direction. This time the suction surface flow acceleration occurred almost till the TE (similar to $\Delta\gamma = 0°$, $\tau/ch = 2.7\%$ case) promoted by the high streamwise component of the tip leakage flow. Hence its encounter with the TE separated flow did not result in further complex interaction of with the tip clearance flow. Instability is thus not observed. Instead, distinct blockage regions corresponding to tip leakage vortex and the TE separation vortex are observed.

At $\Delta\gamma = +5°$, Various Tip Gaps

In a higher stagger angle case, $\Delta\gamma = +5°$, $\tau/ch = 0.0\%$ (Fig.5a), nature of the separations of the centrifuged blade boundary layer flow is altered from the case with $\Delta\gamma = +3°$, in the same way it was altered when the stagger angle was changed from $\Delta\gamma = 0°$ to $\Delta\gamma = +3°$. The circumferential extent of blockage due to the separated flow is again increased at this higher stagger case $\Delta\gamma = +5°$. Under such

conditions, only a limited portion of the passage near the tip sections is available for the incoming flow progression. Since such portions are close to the mid tip chord portions of the adjacent blades pressure surface (where relatively higher pressures prevail) incoming flow experiences non-favorable pressure gradients in its own direction. In such cases, even a small perturbation may as well lead to self-amplifying instabilities to cause stalling. Such small perturbation could be in the form of a flow instability initiated within the same blade passage - or in the form of an altered mass flow rate due to the incidence implications got from the adjacent passage - or spanwise redistribution of flow.

When the tip clearance of $\tau/ch = 0.7\%$ is introduced (Fig.5a), the flow structure is similar to that at $\Delta\gamma = +3°$, $\tau/ch = 0.7\%$ with hints of similar instability conditions. Flow acceleration on the suction surface in front parts of the blade is less in higher stagger angle cases due to low streamwise velocity of the flow. Tip leakage is found to be more perpendicular to the chord in these cases, implying that the leakage is more "axially backward" in nature. For this reason reduced velocities near the LE plane are observed due to more axially reversed tip leakage flow, contributing additional blockage in these regions, while at low stagger angles, the leakage flow had complemented the flow acceleration in these regions, close to the LE.

At a higher clearance ($\tau/ch = 2.7\%$), a complete breakdown of the flow field can be seen. The whole flow passage is observed to cease out for the flow progression with the axially reversed flows and the tip leakage flow. A noticeable instability is clearly seen (shown as *I-2* in Fig.5a) close to the leading edge of the tip leakage vortex. A local flow recirculation around this instability can be seen and the axially reversed flow at the blade TE spreads in the circumferential direction. Passage close to the tip is completely blocked for the flow progression over the whole circumferential extent. Magnified views of *I-1* and I-2 are provided in Fig.6 for better depictions.

Flow at the Blade Suction Surface Hub Endwall Corner

Figures 7a - 7c show close views of flow pictures near the blade TE - hub endwall corners. These figures are plotted with velocity vectors and hypothetical surface streamlines colored with axial velocity coefficient to provide clear pictures. Passage vortex (PV) appears in a giant size in these highly magnified figures. Corner formed by the blade suction surface and the hub endwall at the hub trailing edge is the present region of interest. Effective negative dihedral that the AXS rotor has with respect to the hub endwall is seen to promote the formation of a corner vortex (CV) in these regions. TCS rotor features little positive dihedral at hub when compared with the UNS rotor. There are no signs of CV formation at the hub TE corner in the TCS rotor.

When the stagger angle is increased to $\Delta\gamma = +3°$ (Fig.7b), a clear picture of CV is seen with the UNS rotor as well as the AXS rotor. TCS rotor does not feature such vortex. At a higher stagger angle $\Delta\gamma = +5°$ (Fig.7c), the corner vortex (CV) still grows larger in UNS and AXS rotors, while the effective local positive dihedral in the TCS rotor, complemented by the high mass flows in these regions acquired from the spanwise flow redistribution still prevents its formation. Local positive dihedral at the blade endwall corners is thus found thoughtful to prevent the formation of such secondary flows. It is clear that the TCS rotor (positive dihedral) features no CV; in the UNS rotor (baseline blade) CV is significant; and in the AXS rotor (local negative dihedral), CV is very much comparable with the PV in terms of size. Indeed, CVs observed in these cases feature high axial velocity deficits on the local flow field indicating high blockages and potential loss to the rotor performance.

Note that all hub trailing edges are aligned at the same distance from the left-bottom-ends of these figures for all rotors. Dotted lines joining centers of the PVs with the hub TE corners, and the dotted lines drawn from the centers of the PVs perpendicular to the blade/endwall surfaces give information regarding how close the PV is located with respect to the blade/endwall when it leaves the blade passage. As a common observation at all stagger angles, PV is closer to the blade in both the swept rotors when compared with that in the UNS rotor. This may not be a critical parameter to influence the flow field, unless some additional installments on the blade/hub endwall such as bleed slots, cooling holes, fences and so forth are made. Shape of the PV in the UNS rotor is observed to be more elliptic while it is comparatively circular in the swept rotors.

Flow Evolution at the Rotor Exit

Contours of some flow parameters (total pressure rise coefficient, static pressure rise coefficient, axial-radial-and-tangential velocity coefficients) and hypothetical surface streamlines are plotted (Fig.8) on a plane which is very close to the TE of the rotor at a distance of 9 mm from

the TE at the hub. These results pertain to the UNS rotor, $\Delta\gamma = +3°$, $\tau/ch = 0.7\%$, representing flow features of the baseline rotor for moderate stagger increment and for moderate tip clearance. This plane is located at a streamwise station where the flow just exits the rotor passage, to appreciably realize various causes resulting in the final flow picture. As the flow progresses downstream to the rotor exit measuring plane, sufficient mixing occurs within the flow and different zones of the flow field merge together obscuring the information on the individual causes.

Flow separation vortex (SV) at the tip trailing edge is indicated in the streamline plot (Fig.8a) as SV enclosed with a dashed circle. Any streamwise vortex of this sort can be confirmed with a radial velocity contour (Fig.8e) in which either sides of the vortex would have radially opposite velocity components. Since no such noticeable signs are seen in this figure for tip clearance vortex, it can be understood that the tip leakage vortex has been mixed out considerably with the throughflow as it reaches this downstream streamwise location.

Observing the total pressure rise coefficient contour (Fig.8b) in comparison with the contours of static pressure rise coefficient and axial velocity coefficient (Fig.8c and 8d) gives clear understanding of pressure rise distribution along with mass flow distribution contribution to the "accountable" pressure rise. Separation Vortex (SV) is found to influence the pressure field local to the casing with a distortion. In these regions, static pressure rise is reasonably high to hold up this high total pressure rise. In the axial velocity contour, regions close to the casing endwall with very low axial velocity coefficient values, as well as with low pressure rise can be better understood as the effect of separated flow from the tip TE; and partially due to the casing wall boundary layers.

Majority of the flow blockage on this plane is due to these secondary flows and the wake. In the radial velocity contour (Fig.8e), SV can be confirmed. Passage vortex can be clearly seen in the streamline plot (Fig.8a) indicated as PV at the hub trailing edge, while signs of such vortex on radial velocity coefficient contour are not clear (weak vortex). Local distortion of wake as influenced by the passage vortex can be observed in Fig.8a. Pressure side of the blade below the midspan features radially inward velocity; and the very adjacent regions feature high radially outward velocity (boundary layer centrifugation) implying high amounts of shear in the wake region. Relative tangential velocity coefficient contours (Fig.8f) show the extent of flow deflection, decreasing from hub to the tip, in accordance with the rotor design [19].

Total pressure rise coefficient contours at the rotor exit are shown in Fig.9. The tip end of the wake features a distinctive zone of low pressure rise. These zones refer to core of the SV. At $\Delta\gamma = 0°$, these zones are very close to the casing endwall. As the stagger angle is increased, these zones got shifted radially inward; with high pressure rise flow occupying the top portions. Various regions in these contours have been tagged: Leakage Vortex (LV), Separated Vortex (SV), and Passage Vortex (PV). It was reported [4] that at high stagger angles leakage vortex forms at forward chordwise locations close to the tip LE; and as it reaches the rotor exit, its core moves radially inward and spreads radially. High pressure flow near the casing after the downstream edge of the leakage vortex pushes the SV radially inward and occupies the upper portions. These regions can be seen in the figure ($\Delta\gamma = +5°$ case) above the Separated Vortex (SV) locations. Note that these high pressure regions close to the casing also suffer from strong axial velocity deficits due to severe blockage caused by the upstream leakage vortex. Such flow blockage is further carried to the downstream stator, and Fig.10a - 10c would facilitate understanding such effects.

Meridional Contours of Axial Velocity Coefficient

Contours of axial velocity coefficient are plotted on meridional planes from the inlet of the rotor to the exit of the stage as shown in Fig.10a - 10c. At every location on these meridional planes axial velocity coefficient is circumferentially mass averaged. These contours are plotted for the near stall mass flow rates at the respective stagger angle cases.

Dark red zones in the forward portions indicate the flow acceleration at the leading edge. These zones thus signify the orientation of the blade LE in various swept rotors. Similar regions can also be observed near the stator LE as well. Positions of rotor and stator are marked with dashed lines in the figures for better clarity (rotor tip gaps have not been depicted in these rough representations). Dark blue zones in these contours depicting the low axial velocities represent the flow blockage. Such regions near the casing are due to separated flow related blockage for zero tip clearance case; and chiefly due to the tip leakage vortex related flow blockage as the clearance is increased.

While high blockage observed in front of the hub LE in the 20° TCS rotor confirms the high incidence in these regions as reported earlier [17]; high blockage near the hub TE of the other two sweep configurations (UNS and 20° AXS) confirms the flow weakness of those rotors near the hub. This is especially significant in case of the 20° AXS rotor. Hub-ward deflection of mean streamlines causes increased mass flow in the TCS rotors avoiding such axial velocity deficits at the hub towards the passage exit. Axial velocity near the casing at these locations, on the other hand, compensates for these effects. Higher blockage near the casing at the blade TE regions can be observed in TCS rotor due to this spanwise flow redistribution. The "flow weakness" is further transferred to the downstream stator component, where development of blockage near the hub in the flow direction is clearly seen in the UNS and AXS rotors. This is not observed with the TCS rotor. Increased blockage at the tip can be observed with increasing tip clearance.

Observing Fig.10b and 10c, following remarks can be made with respect to increased stagger angle:

- At higher stagger angles, tip leakage vortex is formed close to the tip LE. Severe blockage can be observed in front of the blade, near the tip due to this reason. At $\Delta\gamma = 0°$, for maximum clearance case ($\tau/ch = 2.7\%$), leakage vortex related flow blockage is confined to regions within the passage only. With increasing stagger angle, this blockage is spread and extended to portions in front of the blade hinting highly increased flow incidence at the passage entrance. Radial spread of the leakage vortex related blockage is also higher at higher stagger angles.
- Spread of low axial velocity regions near the hub TE also increases with increasing stagger angle. When the stagger angle is increased, all the blade sections are rotated by the same amount to close the passage. However, portions at low radii close quicker than those at the high radii; and thus is this effect. On the other hand, large cross flows in the hub endwall were already observed (and discussed in the previous sections) at higher stagger cases towards the stall mass flow rates due to high loading with low streamwise velocities. These cross flows resulted in the formation of a corner vortex at the blade suction surface hub endwall corner, depending on the severity of cross flows and local flow conditions.

Summary and Conclusions

This paper addresses two critical aspects of the endwall flow structure in a subsonic axial flow compressor: flow mechanism leading to stalling at different stagger angle configurations; and the effect of tip leakage flows on these flow phenomena. Hub endwall flow structure and the downstream flow evolution have also been discussed, however in less detail. The following salient conclusions have been made:

- Stagger angle has significant effect on suction surface flow separations. At higher stagger angles, much of the flow centrifugation is commenced at early chordwise locations on the blade and it is nearly radial at these portions. This resulted in two distinct separation zones on the suction surface, one at an early chordwise location near the middle of the tip chord and the other towards the tip trailing edge at higher stagger angles.
- Due to the upstream shift of the separation regions on the suction surface with increased stagger angle, introduction of little clearance at the tip had a beneficial effect for certain stagger angle increments owing to beneficial interaction of tip leakage flows with the flow field local to the tip regions. However, the separated flow at high stagger angles was found to grow in size leaving very little room for flow progression. This resulted in the incoming flow to experience hostile pressure conditions in its own direction. Under these conditions, even a small perturbation could lead to self-amplifying instabilities causing stalling. Large tip gaps therefore become critical at high stagger angles, as the leakage flow along with the prevailing severe secondary flows occupies larger circumferential extents resulting in severe flow blockage; and found to give rise to instabilities.
- At higher stagger angles, stall point shifts towards the low mass flow rates with similar or higher total pressure rise. This results in higher cross flows especially near the hub endwall, due to the prevailing higher pitchwise pressure gradients with low streamwise velocities. These secondary flows were less severe in tip chordline swept rotors.
- Hub ward flow weakness has been observed with unswept and axially swept rotors, which was found to be further carried to the downstream stator component.

References

1. Ramakrishna, P. V. and Govardhan, M., "Combined Effects of Forward Sweep and Tip Clearance on the Performance of Axial Flow Compressor Stage", Proceedings of the ASME Turbo Expo, Orlando, Fla, USA, GT2009-59840, 2009.

2. Ramakrishna, P. V. and Govardhan, M., "Study of Sweep and Induced Dihedral Effects in Subsonic Axial Flow Compressor Passages - Part II: Detailed Study of the Effects on Tip Leakage Phenomena", International Journal of Rotating Machinery, Vol.2010, Article ID 491413, 13 Pages, 2010.

3. Yoon, Y.S., Song, S. J. and Shin, H. W., "Influence of Flow Coefficient, Stagger Angle, and Tip Clearance on Tip Vortex in Axial Compressors," Journal of Fluids Engineering, Vol.128, No.6, pp.1274-1280, 2006.

4. Ramakrishna, P.V. and Govardhan, M., "Effect of Tip Clearance on the Performance of Forward Swept Subsonic Axial Compressor Rotors at High Stagger Angles", Proceedings of the ASME International Mechanical Engineering Congress and Exposition (IMECE2011), Denver, Colorado, USA, IMECE2011 - 65103, 2011.

5. März, J., Hah, C. and Neise, W., "An Experimental and Numerical Investigation into the Mechanisms of Rotating Instability", ASME Journal of Turbomachinery, Vol.124, No.3, pp.367-375, 2002.

6. Mailach, R., Lehmann, I. and Vogeler, K., "Rotating Instabilities in an Axial Compressor Originating from the Fluctuating Blade Tip Vortex", ASME Journal of Turbomachinery, Vol.123, pp.453-463, 2001.

7. Zierke, W.C., Farrell, K.J. and Straka, W.A., "Measurement of the Tip Clearance Flow for a High-Reynolds-Number Axial-flow Rotor", ASME Journal of Turbomachinery, Vol.117, pp.522-532, 1995.

8. Hoying, D.A., Tan, C.S.., Vo, H.D. and Greitzer, E.M., "Role of Blade Passage Flow Structures in Axial Compressor Rotating Stall Inception", ASME Journal of Turbomachinery, Vol.121, pp.735-742, 1999.

9. Wisler, D.C., "Core Compressor Exit Stage Study, Volume IV - Data and Performance Report for the Best Stage Configuration, NASA CR-165357, 1981.

10. Silkowski, P.D., "Measurements of Rotor Stalling in a Matched and a Mismatched Multistage Compressor", GTL Report, 221, Gas Turbine Laboratory, Massachusetts Institute of Technology, 1995.

11. Davis, R.L. and Yao, J., "Axial Compressor Rotor Flow Structure at Stall-inception", Proceedings of AIAA Aerospace Sciences Meeting and Exhibit, AIAA 2006-419, 2006.

12. Suder, K.L. and Celestina, M.L., "Experimental and Computational Investigation of the Tip Clearance Flow in a Transonic Axial Compressor Rotor", NASA Technical Memorandum, TM-106711, 1994.

13. Saathof, H., Deppe, A. and Stark, U., "Steady and Unsteady Casing Wall Flow Phenomena in a Single-Stage Low-Speed Compressor at Part-Load Conditions", International Journal of Rotating Machinery, No.9, pp.327-335, 2003.

14. Cumpsty, N.A., "Part-Circumference Casing Treatment and the Effect on Compressor Stall", ASME Paper No. 89-GT-312, 1989.

15. Day, I.J., "Stall Inception in Axial Flow Compressors", ASME Journal of Turbomachinery, No.115, pp.1-9, 1993.

16. Saathoff, H. and Stark, U., "Tip Clearance Flow iNduced Endwall Boundary Layer Separation in a Single-stage Axial-flow Low-speed Compressor", ASME Paper, 2000-GT-0501, 2000.

17. Ramakrishna, P. V. and Govardhan, M., "Study of Sweep and Induced Dihedral Effects in Subsonic Axial Flow Compressor Passages - Part I: Design Considerations - Changes in Incidence, Deflection, and Streamline Curvature", International Journal of Rotating Machinery, Vol.2009, Article ID 787145, 11 Pages, 2009.

18. Ramakrishna, P.V. and Govardhan, M., "Aerodynamic Performance of Low Speed Axial Flow Compressor Rotors with Sweep and Tip Clearance", Journal of Engineering Applications of Computa-

tional Fluid Mechanics, Vol.3, No.2, pp.195-206, 2009.

19. Ramakrishna, P.V., "Computational Studies on Sweep, Tip Clearance and Stagger Angle Effects in a Subsonic Axial Flow Compressor", Ph.D. Dissertation, Indian Institute of Technology Madras, Chennai, 2011.

20. Krishnakumar, O.G., "Experimental and Computational Studies on Forward Swept Axial Compressor Rotors", M.S. Dissertation, Indian Institute of Technology Madras, Chennai, 2003.

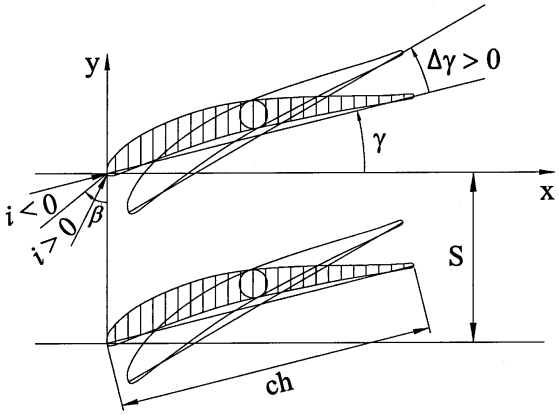

Fig.1 Definition of Stagger and the Conventions

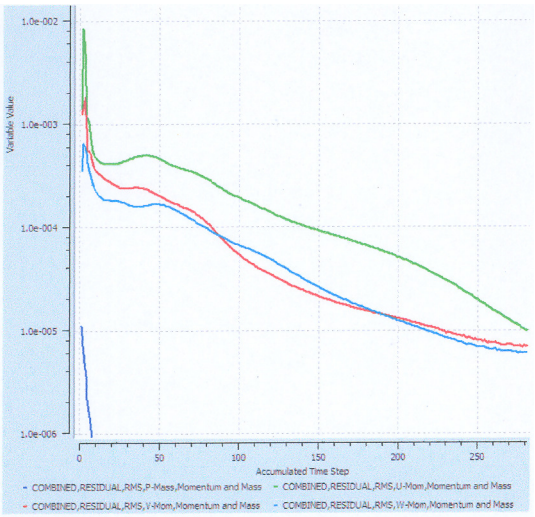

Fig.2a Residual Monitoring Plot of Simulation

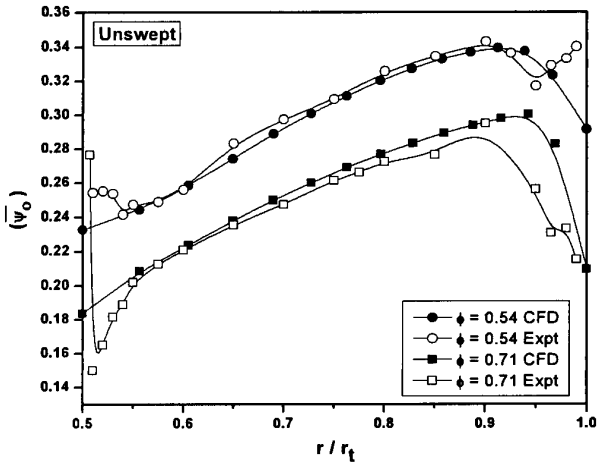

Fig.2b Variation of $\bar{\psi}_o$ at the Rotor Exit

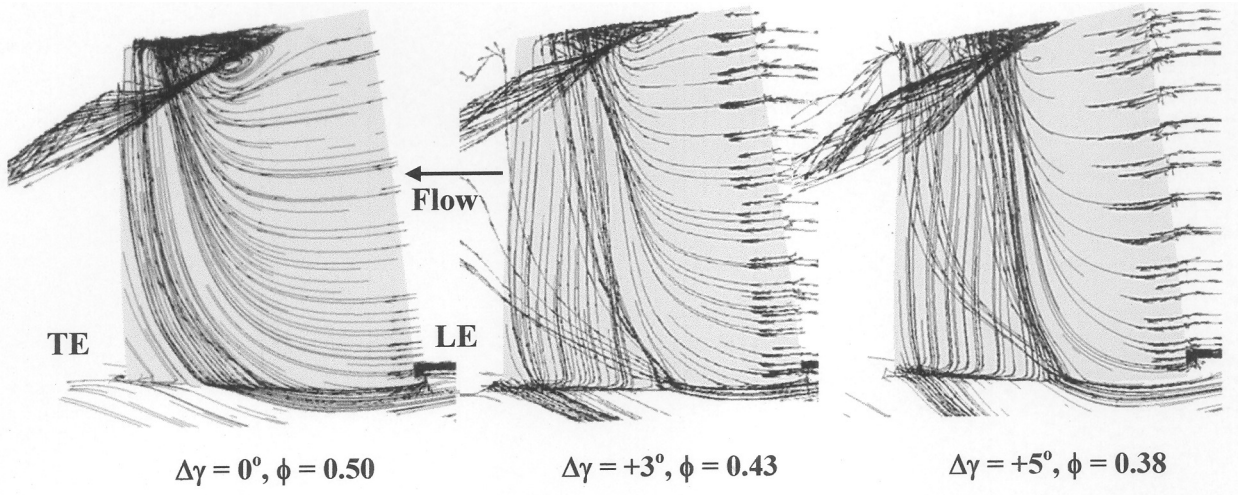

Fig.3 Flow Separation at the Blade Suction Surface

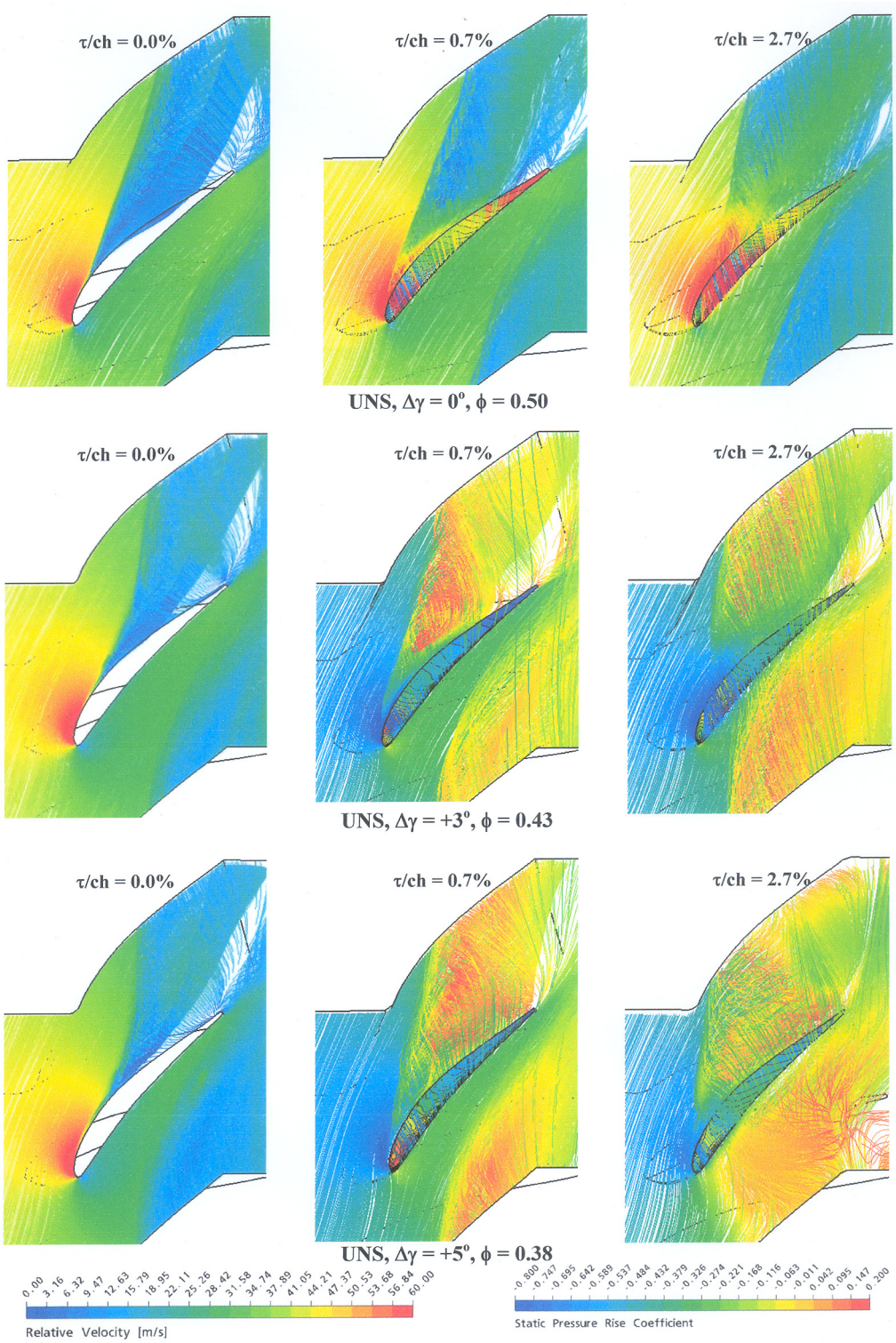

Fig.4 Flow Field Near the Tip with Static Pressure Rise Coefficient Contours

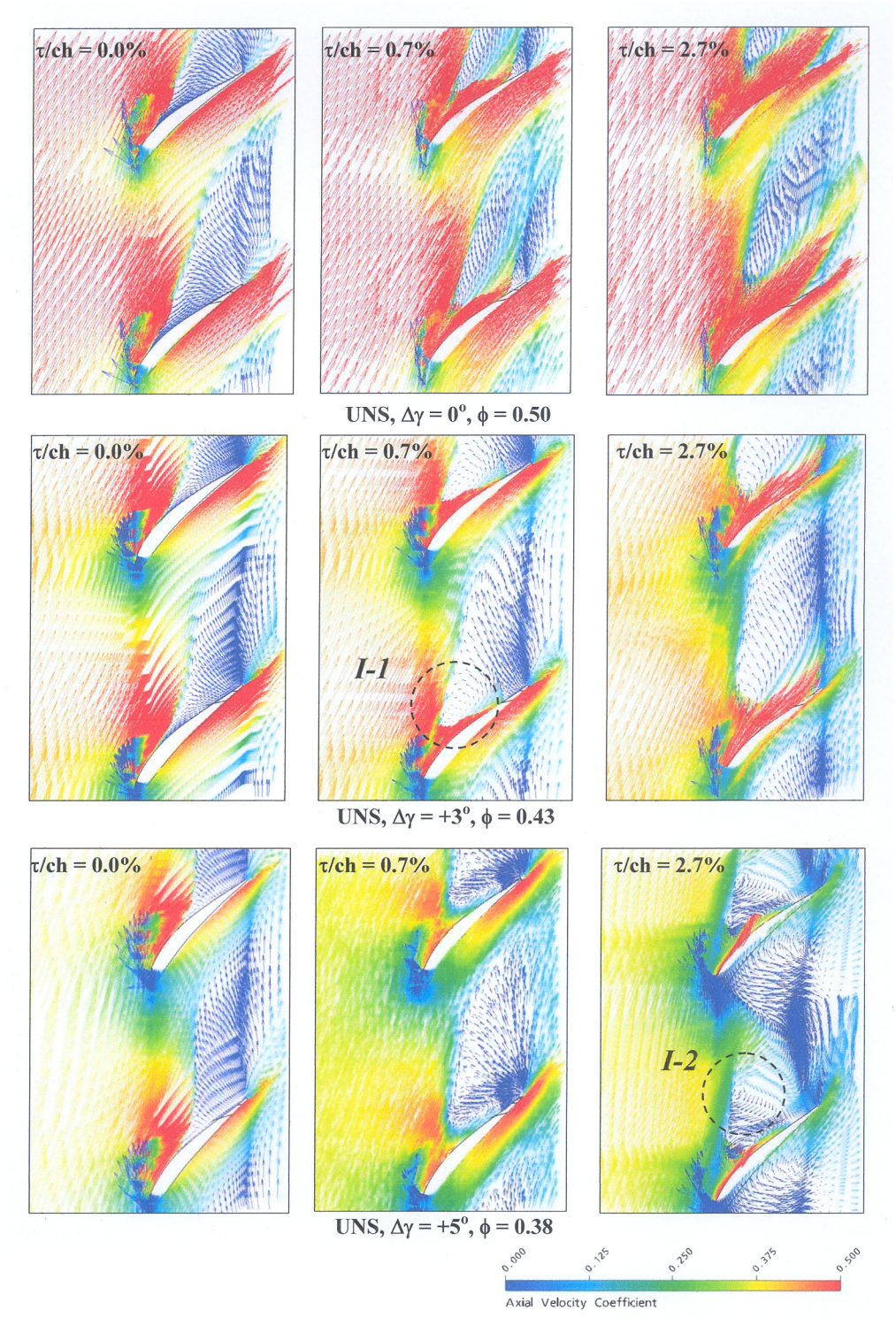

Fig.5a Velocity Vector Field on Blase-to-Blade Plane Coloured with Axial Velocity Coefficient for UNS Rotor

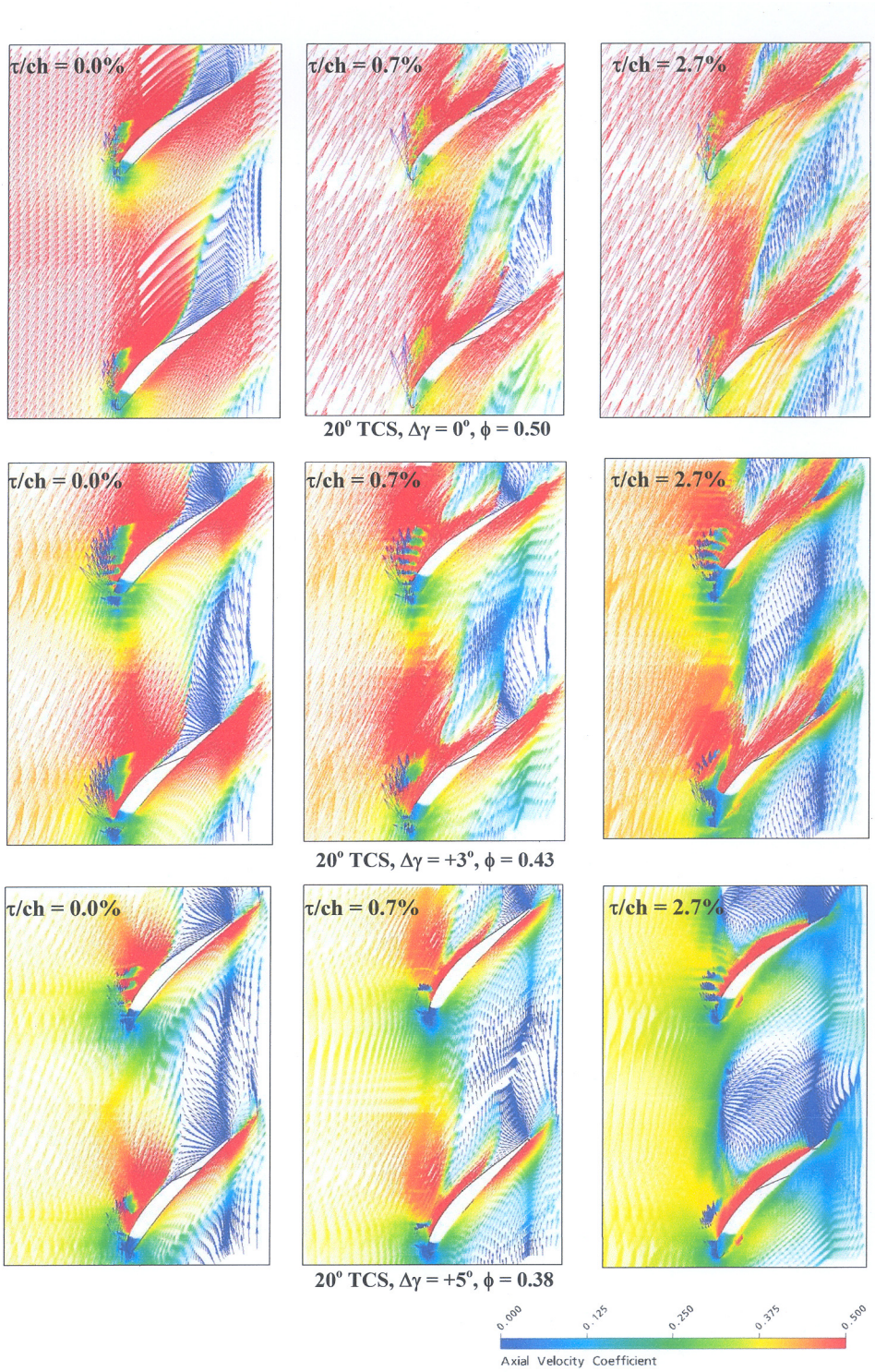

Fig.5b Velocity Vector Field on Blase-to-Blade Plane Coloured with Axial Velocity Coefficient for 20° TCS Rotor

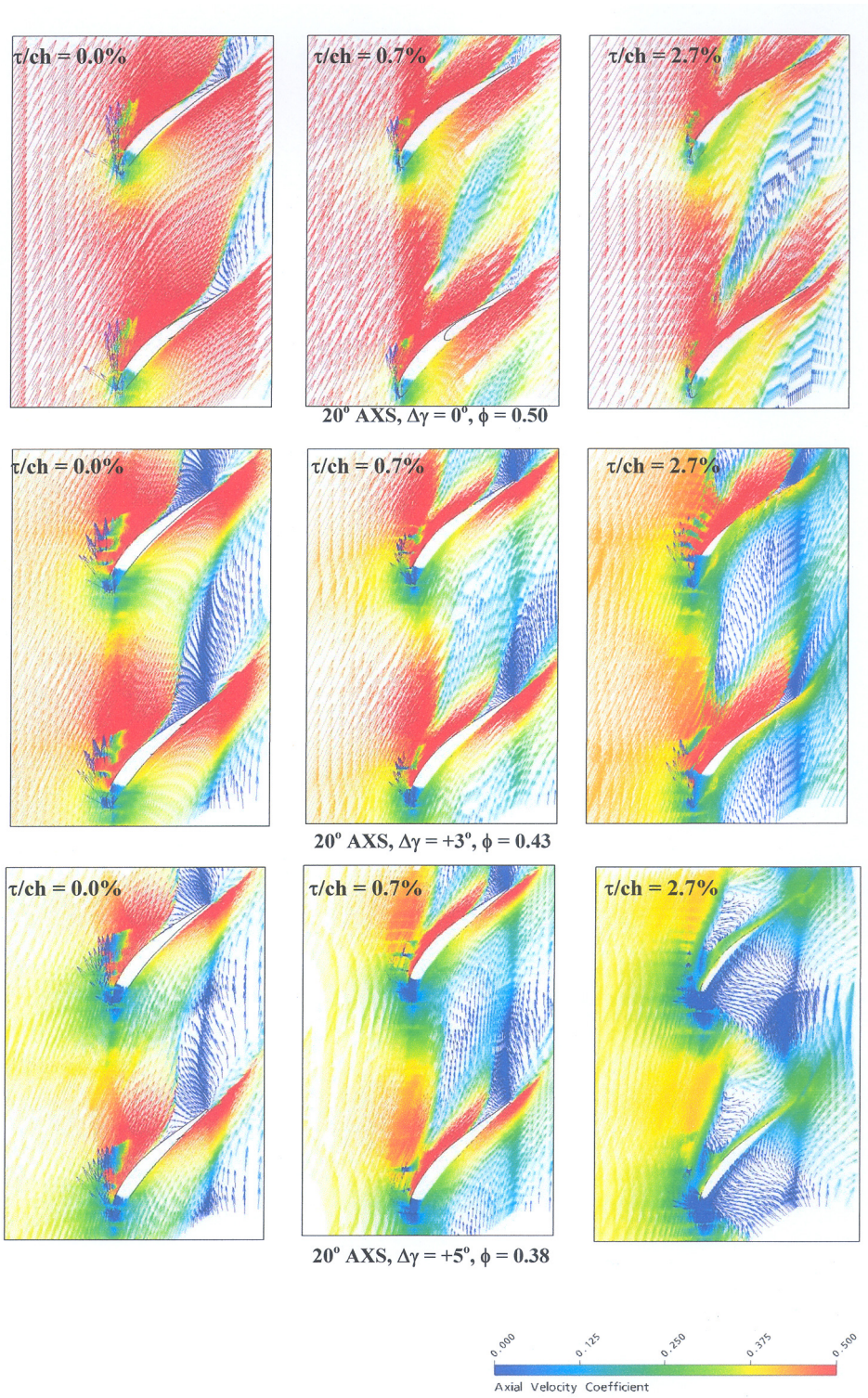

Fig.5c Velocity Vector Field on Blase-to-Blade Plane Coloured with Axial Velocity Coefficient for 20° AXS Rotor

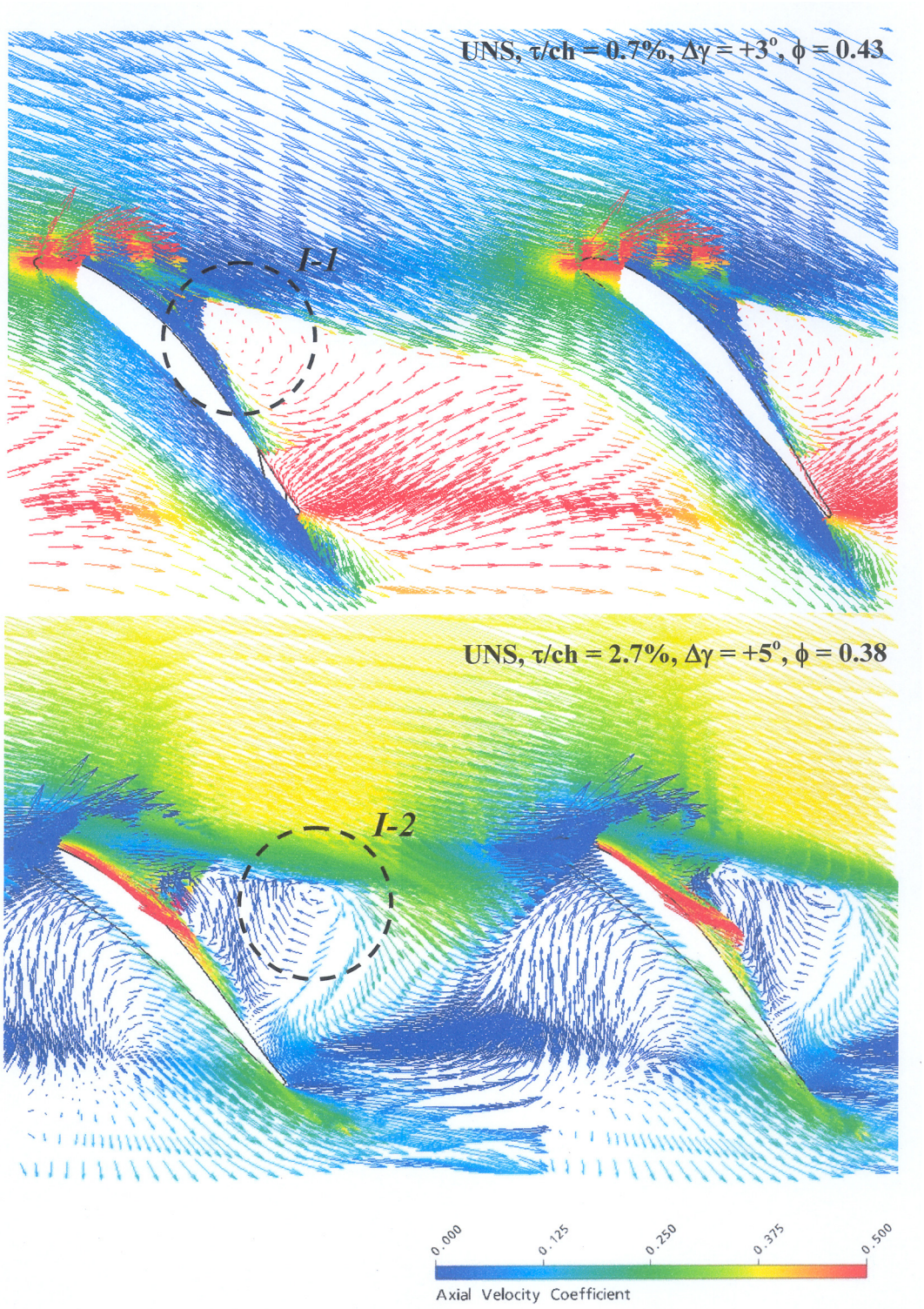

Fig.6 Velocity Vector Field on Blase-to-Blade Plane Coloured with Axial Velocity Coefficient for UNS Rotor

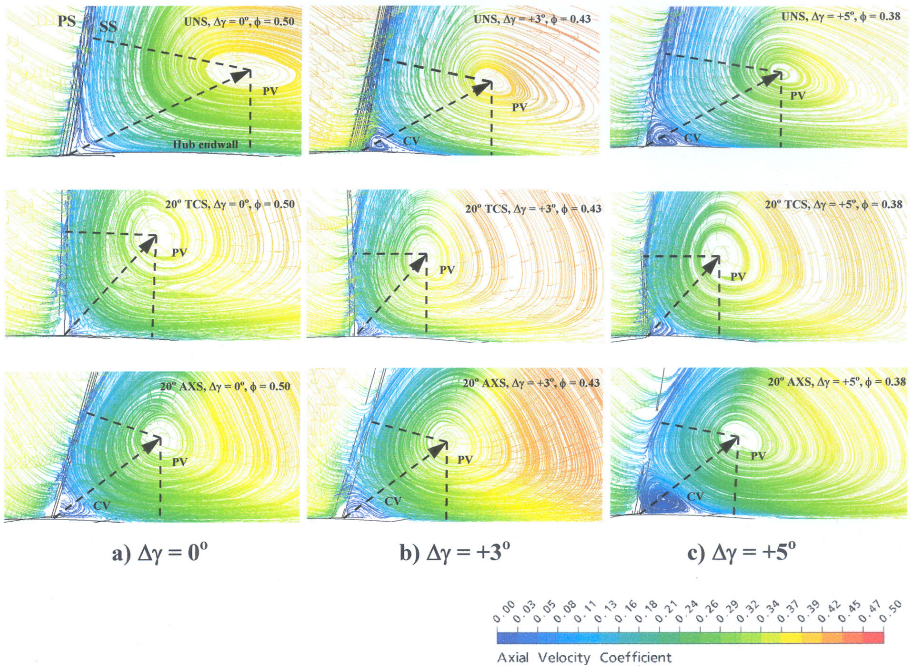

Fig.7 Closed Views of Flow Picture at Blade Hub Trailing Edge Corners

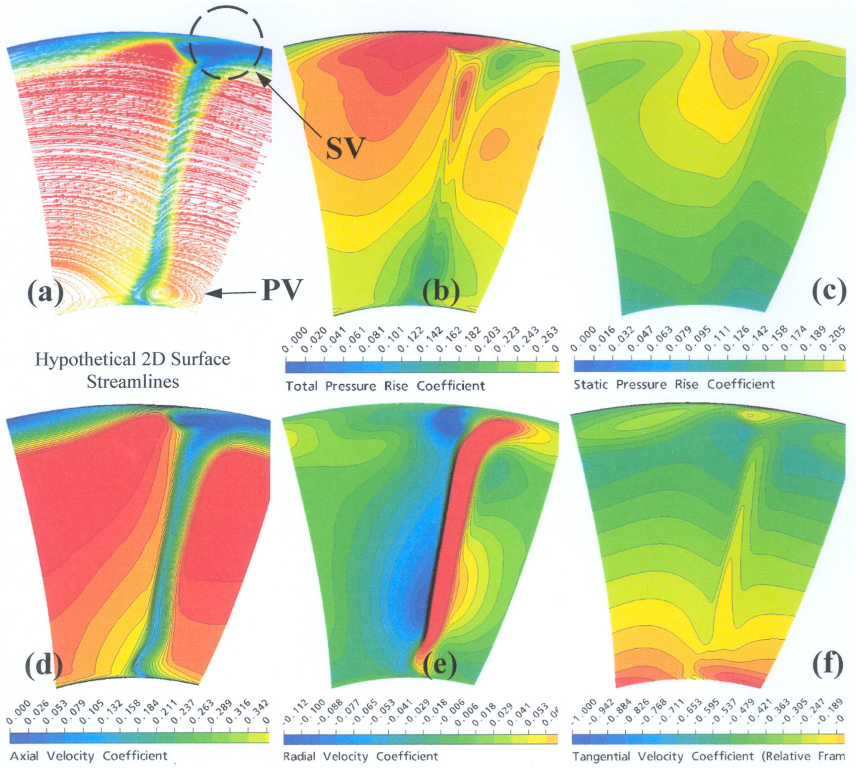

Fig.8 Flow Field Quantities on a Plane Parallel to the TE at the Rotor Exit (x = 0.98) for UNS, Δγ = -3°, τ/ch = 0.7%)

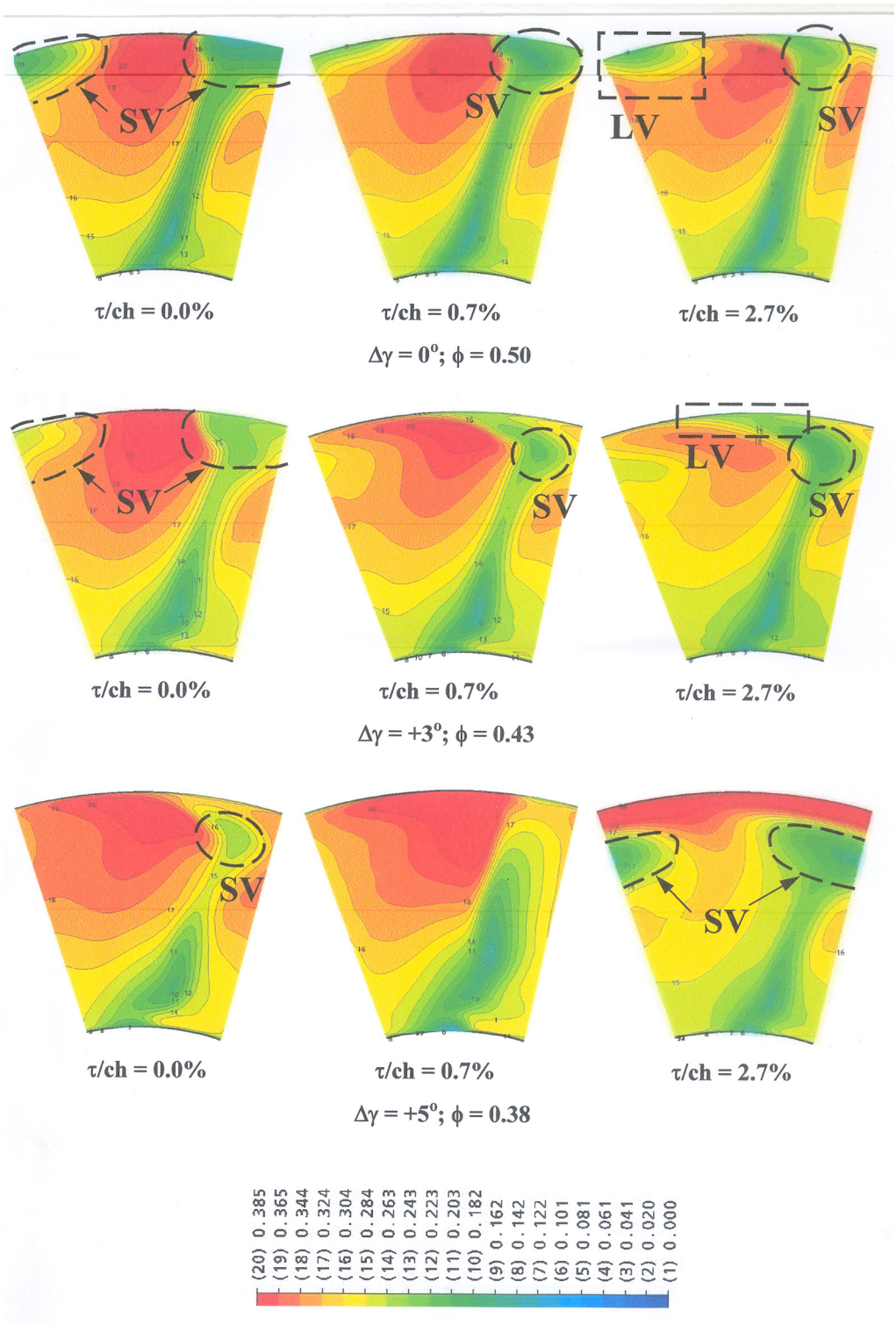

Fig.9 Contours of Total Pressure Rise Coefficient at the UNS Rotor Exit

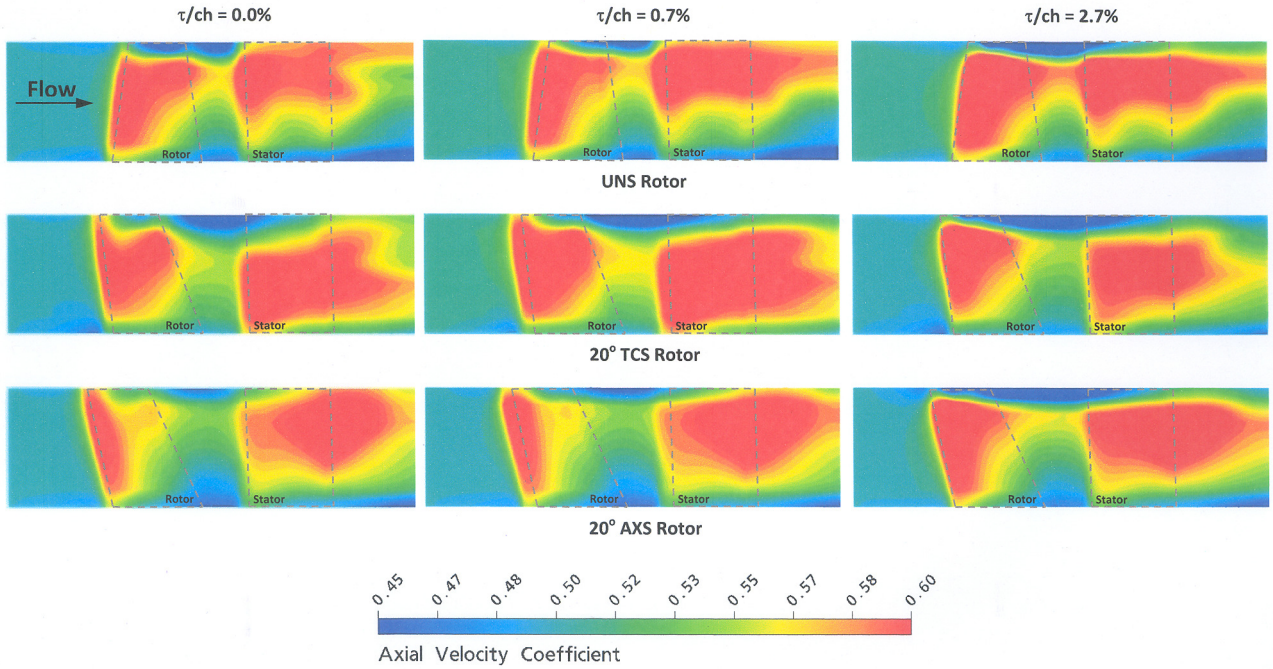

Fig.10a Distribution of Axial Velocity Coefficient on the Meridional Plane for $\Delta\gamma = 0°$, $\phi = 0.50$

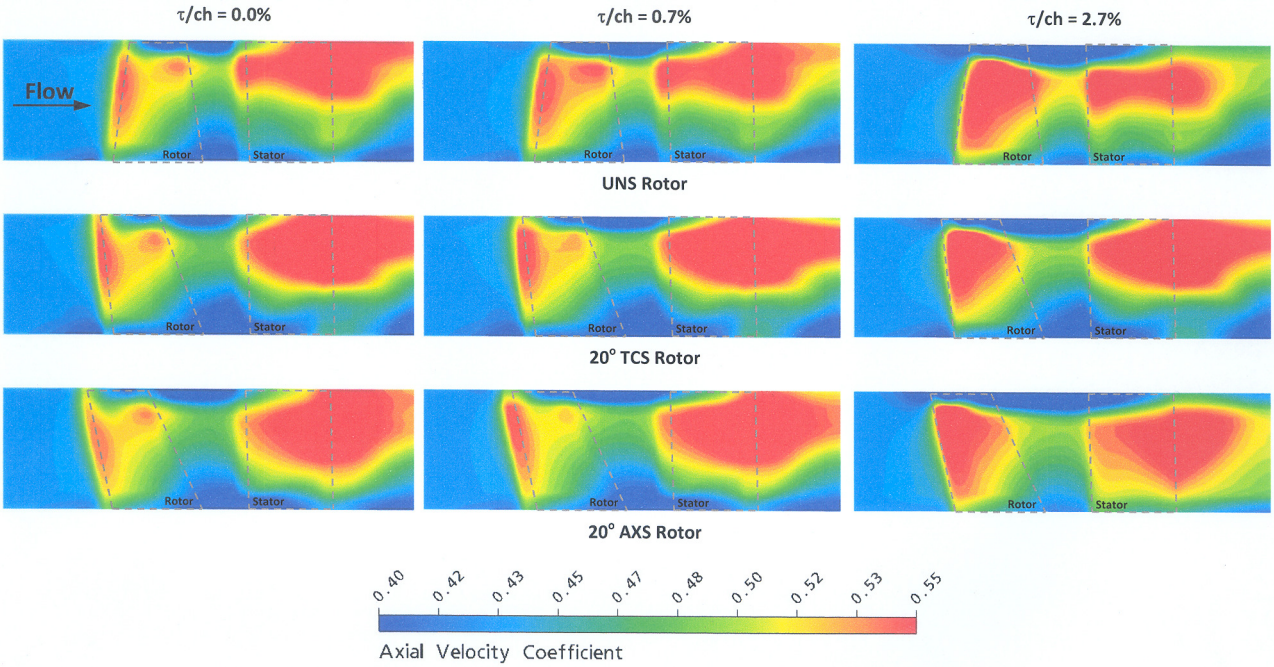

Fig.10b Distribution of Axial Velocity Coefficient on the Meridional Plane for $\Delta\gamma = 3°$, $\phi = 0.43$

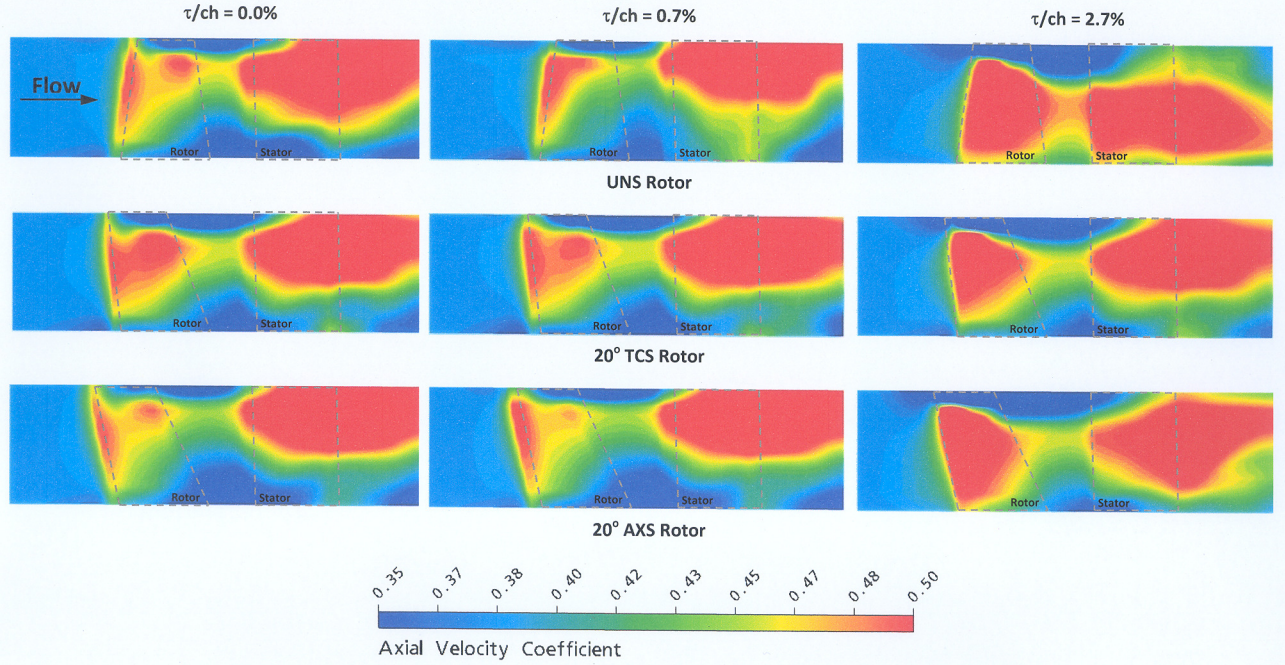

Fig.10c Distribution of Axial Velocity Coefficient on the Meridional Plane for $\Delta\gamma = 5°$, $\phi = 0.38$